 doi:10.20944/preprints202102.0565.v1

Article

Effects of mesh generation on modeling aluminum Anode Baking Furnaces

Jose Libreros [1†,*], Domenico Lahaye [2†] and Maria Trujillo [3†]

[1] School of Systems Engineering and Computing, Universidad del Valle, Ciudad Universitaria Meléndez, Calle 13 No 100-00, 760032, Cali, Colombia; jose.libreros,maria.trujillo@correounivalle.edu.co
[2] Delft Institute of Applied Mathematics. Building 28. Mourik Broekmanweg 6 2628 XE Delft, The Netherlands; D.J.P.Lahaye@tudelft.nl
* Correspondence: jose.libreros@correounivalle.edu.co
‡ These authors contributed equally to this work.

Abstract: Turbulent flow is the first and fundamental physical phenomena to evaluate when optimising cost and reducing emissions from an Anode Baking Furnace (ABF). Gas flow patterns, velocity field, pressure drop, shear stress, and turbulent dissipation rate variables are the main operational parameters to be optimised, considering a specific geometry. Computational Fluid Dynamics (CFD) allows simulating physical phenomena using numerical methods with computer resources. In particular, the finite element method is one of the most used methods to solve the flow equations. This method requires a discretisation of the geometry of the ABF, called mesh. Hence, mesh is the main input to the finite element method. A suitable mesh for applying a discretisation method determines whether the problem can be simulated or not. Generating an appropriate mesh remains a challenge to perform accurate simulations. In this work, a comparison between meshes generated using two mesh generation tools is presented. Results of different study cases are included.

Keywords: Anode Baking Furnaces; turbulence flow model; mesh generation; Computational Fluid Dynamics

1. Introduction

Aluminium anodes are the significant components in the extraction process of aluminium from bauxite ore in 15% and therefore, are considered essential [1]. Anodes are baked (heat-treated) in advance to obtain particular mechanical, thermal and electrical properties that make them suitable to be used in the aluminium production process. Anode baking is carried out in an open-top ring-type furnace, called Anode Baking Furnace (ABF).

In a general way, anodes are baked by heating the refractory walls. This process is performed by direct gas injection from the top of the furnace [2]. The anode baking generally takes 390-480 hours, and several phenomena occur during this process; such as gas flow, velocity, pressure, and shear stress patterns. Such phenomena are a base of subsequent chemical and heat phenomena.

Anode baking requires a vast amount of energy and releases undesired gases such as NOx. According to new environmental regulations, it is required to set new parameters that allow reducing NOx [3]. Aerodynamic studies serve as an opportunity for refinement since emissions are caused by flow interactions. [4].

Therefore, an ideal anode baking process requires optimisation in reducing NOx, soot-free combustion, reduction of energy utilisation and improving quality of anodes.

Research *in situ* on the effects of operational and geometrical parameters on the performance of the furnace is not operationally feasible. In particular, guaranteeing improvement results within environmental requirements by plant tests is usually expen-

 doi:10.20944/preprints202102.0565.v1

sive and disrupt a baking process. Moreover, design an anode baking furnace with no background is a difficult and time-consuming task.

Instead, numerical-mathematical modelling is an imperative approach to study the effect of different parameters on anode quality and furnace performance. Ultimately, the optimum baking process and furnace geometry can be proposed [5]. Generally, anode baking furnaces are designed, remodelled and improved by extrapolation from existing furnaces. Computational Fluid Dynamics (CFD) are the preferred technique to modelling.

CFD modelling of ABF is based on a typical ABF installation. Fuel is injected according to a specified time-dependent law into burners located at the top of the furnace module. The rate and frequency at which fuel is fed into the burner depend on the specific burner's characteristics, and injection frequency is higher for high-speed burners. The overall effects is that of a pulsating combustion process. Combustion air enters into the furnace through air inlets. Fluid is convected and diffused by the general turbulent flow. As in every process of this kind, the main goal is to ensure flow uniformity inside the furnace for the correct baking of anodes, considering subsequent phenomena.

CFD modelling uses a software-assisted design of the furnace to be considered. This representation is called geometry. Computing has a discrete nature. Hence, designed geometry may be divided into unit controls to perform calculations of the phenomena at each specific location. The result of the division is a discrete grid (called mesh) that can be used as input of the existing methods for numerically solving differential equations, of which consist the most known physical phenomena.

Differential equations that represent the flow of a fluid are well known in the industry and academia for their high complexity due to the presence of non-linear terms. There exists different variations of the government equations that represent different phenomena. Additionally, it is known that very small mesh element sizes are needed to converge to an adequate solution of the differential equations with minimal error. But defining how fine the resulting mesh will be remains an object of study [4,6–8]. Each control unit in all the equations being considered must be solved. Thus, the computational load is higher. Finer meshes imply an unfeasible problem to be solved. In this paper we compare three meshes generated using cfMesh and COMSOL Multyphisics. Nine models were created using different parameters and interchanging meshes. With the aim of reducing the computational load, meshes have defined were defined with a smaller cell size only in critical areas, compared to the rest of the geometry areas, where an adequate modelling with low error and according to reality is achieved. Meshes generated using cfMesh were able to represent better the physical phenomenon.

2. State of the art

This problem has been addressed in the literature by mathematical simulation.

Specific aspects of simulations are reported in [9–11]. Moreover, the mathematical modelling of the anode baking process has been developed and improved significantly in past years. In 1983, Bui et. al. simulated horizontal flue ring furnace in which they treated furnace as a counter-flow heat exchanger [12]. Many models that have been developed at the later stage are based on these early developed models. A more detailed 3D modelling of the ABF started in the mid-90s. Kocaefe et. al. presented a model in which a commercial CFD code CFDS-FLOW3D was used for solving the governing differential equations [13]. However, this model used simplified combustion and radiation models failing to comment on the pollutants.

Severo and Gusberti established a boundary conditions to be able to properly bake all brands of raw materials that may be expected [14]. Moreover, they developed a user-friendly software to analyse furnace energy efficiency, minimum oxygen concentration in different sections [1]. However, for obtaining more specific data related to soot or NOx formation with higher accuracy, the tool cannot be considered.

Preprints (www.preprints.org) | NOT PEER-REVIEWED | Posted: 25 February 2021 doi:10.20944/preprints202102.0565.v1

Ping et al. [15] have reported the effect of baffles and tie bricks arrangements on flow characteristics of anode baking process. From their report, baffles and tie-bricks positioning has a significant impact on flow homogeneity. Ordronneau et al. [16] demonstrated the necessity of employing different simulation tools in meeting the challenge of increasing anode baking furnace productivity.

Other studies have explored deformations of geometry. For instance, Baiteche et al. [17] studied the effect of flue-wall deformation on anode temperature distribution. Comparing the temperature profiles on a line in the pit transverse direction for straight and deformed flue-walls, it was observed that after flue-wall deformation, the temperature profile is no more symmetric which indicates a non-uniform baking process. Later on, Zaidani et al. [18] have also studied the effect of flue-wall deformation on anode temperature distribution.

From experiments, Kocaefe et al. [19] have provided enhanced physical understanding of ABF performance. Enhance performance may be reached by using different computational tools with a different level of complexities. In that way, the $\kappa - \epsilon$ turbulent flow model has a nonlinear behaviour. It represents, in a way, a "worst-case" with demands to nonlinear iterations [20]. This work has findings that the Reynolds Averaged turbulent Navier-Stokes equations can be solved by a Newton iterative process after finite element discretization with the distinct advantage of the superlinear convergence over traditionally used SIMPLE-based approaches.

A dynamic process model was developed by Oumarou et al. to investigate the effect of temperature variation in the vertical component by considering a vertical component of flue gas [21–23]. This allows the 2D temperature distribution boundary condition for the pit sub model. However, the model fails to optimize reducing emissions, saving energy and maintaining anode quality.

A similar work is carried out by Tajik. et. al. in which effect of flue wall design on the flow field, combustion and temperature has been modelled in Ansys Fluent [24,25]. The finite volume method is used in Ansys Fluent. Whereas, COMSOL®Multiphysics is based on the finite element method. It would be interesting to compare the results with two approaches. In conclusion, vast modelling approaches are developed for anode baking furnace. However, the model for NOx reduction still needs significant attention.

Chaodong et al. [26] have used a finite element method (FEM) based model with the aim of developing a large scale, high efficiency and energy saving baking furnace. They reported results with two proposed designs. The reported designs have been optimised for the flue-wall and exhaust ramp. Gaoui et. al. [27] have examinated the influence of baffles. The idea was to remove the baffles and simulating using finite element method. Some pitfalls were found on the road like uneven heat distribution, too fast degassing or fluewall pinching.

Nakate et al. [7] have developed a model that focuses on reducing NOx emissions. First, they developed the turbulent flow. Then, the model have been extended by adding combustion reaction. As a third step, heat transfer have been considered in the general model. However, the software used is constrained by the basic eddy dissipation model. It is necessary to have detailed combustion models based on probability density function.

A bottom-up study has perfomed previously [8]. Firstly, models were simulated using 2D geometry. This implies no consideration of $z-$component. Modelling in two dimensions allows to have familiarisation with the model and extract general flow features inside the furnace. Modelling in two dimensions allows to describe turbulence behaviour in one planar surface. They used the Spalart Allmaras one-equation model. Later, authors developed the model using three dimensions [28]. Moreover, they did analysis of fluid flow using a more-realistic represented geometry at the burner zone. Unike [8], two-equation Realizable ϵ model were considered. Standard Wall Functions are used at all solid walls. In this study, they concluded that using two dimensions has a high contribution of the $z-$component to a well-described fluid flow [28]. They propose that the conflict between the physical behaviour of the flow and the prescribed uniform

Preprints (www.preprints.org) | NOT PEER-REVIEWED | Posted: 25 February 2021 doi:10.20944/preprints202102.0565.v1

value for pressure can have detrimental numerical effects. Numerical impact could occur when slowing down or simply making impossible to reach the full convergence of the numerical method. For that reason they proposed that outlet zones may be redesigned to ensure flow uniformity.

Additionally, there are reports about other physical phenomena. Grégoire et al. [29] conducted a comparative study on two different modeling approaches for anode baking furnace combustion modeling. In a report by Grgoire and Gosselin, a comparison of three combustion models for anode baking furnace is carried out in Ansys Fluent [30].

Table 1 provides a summary of the recent literature.

In this work, we focused on examining the turbulent flow patterns as one of the aspects mentioned to be optimised. In particular, we examine the effect of using three different meshes as input of the finite element method.

3. Model description

In this section, mathematical fundamentals are presented, more detailed can be found in Wilcox [31].

Standard $k-\epsilon$ turbulence model

The following equations are solved for the 6 unknown parameters (p, $\overline{u_1}$, $\overline{u_2}$, $\overline{u_3}$, k and ϵ) during the incompressible isothermal flow computation:

$$\frac{\partial \overline{u_j}}{\partial x_j} = 0 \tag{1}$$

$$\overline{u_j}\frac{\partial \overline{u_i}}{\partial x_j} = -\frac{\partial \tilde{p}}{\partial x_i} + \frac{\partial}{\partial x_j}\left[\nu_{eff}\left(\frac{\partial \overline{u_i}}{\partial x_j} + \frac{\partial \overline{u_j}}{\partial x_i}\right)\right], \quad i, = 1,2,3 \tag{2}$$

$$\overline{u_j}\frac{\partial k}{\partial x_j} = \frac{\partial}{\partial x_j}\left[\nu^k_{eff}\frac{\partial k}{\partial x_j}\right] + \nu_T\frac{\partial \overline{u_i}}{\partial x_j}\left(\frac{\partial \overline{u_i}}{\partial x_j} + \frac{\partial \overline{u_j}}{\partial x_i}\right) - \epsilon \tag{3}$$

$$\overline{u_j}\frac{\partial \epsilon}{\partial x_j} = \frac{\partial}{\partial x_j}\left[\nu^\epsilon_{eff}\frac{\partial \epsilon}{\partial x_j}\right] + C_{1\epsilon}\frac{\epsilon}{k}\nu_T\frac{\partial \overline{u_i}}{\partial x_j}\left(\frac{\partial \overline{u_i}}{\partial x_j} + \frac{\partial \overline{u_j}}{\partial x_i}\right) - C_{2\epsilon}\frac{\epsilon^2}{k} \tag{4}$$

$$\nu_{eff} = \nu + \nu_T \tag{5}$$

$$\nu^k_{eff} = \nu + \frac{\nu_T}{\sigma_k} \tag{6}$$

$$\nu^\epsilon_{eff} = \nu + \frac{\nu_T}{\sigma_\epsilon} \tag{7}$$

$$\nu_T = C_\mu\frac{k^2}{\epsilon + \epsilon_s} \tag{8}$$

$$\sigma_k = 1 \quad \sigma_\epsilon = 1.3 \quad C_\mu = 0.09 \quad C_{1\epsilon} = 1.44 \quad C_{2\epsilon} = 1.92. \tag{9}$$

The laminar viscosity μ is calculated using Sutherlands's law $\mu = A_s\frac{T^{3/2}}{T+T_s}$ where $A_s = 1.67212E^{-6}$, T_s = 170.672 are constants.

The over-bar denotes the ordinary reynolds averaging.

4. Model configurations

The comparison of meshes is done along with varying parameter as describing in Table 2. We use COMSOL Multiphysics for solving the Navier-Stokes $\kappa-\epsilon$ turbulence model. All solver parameters are set as default except for linear solver. For linear solver,

Preprints (www.preprints.org) | NOT PEER-REVIEWED | Posted: 25 February 2021 doi:10.20944/preprints202102.0565.v1

Table 1. Summary of literature review on ABF desing modelling

Authors	Year	Objectives	Combustion model	Detailed kinetics	Radiation model
Ping. et al.	2002	Influence of the baffles on flowing field	Non-reactive flow	Not included	Not included
Severo et al.	2005	Developing a 3D CFD model for Flue-wall design modification	EDM	Not included	P1
Ordronneau et al.	2006	Application of CFD simulation for crossover design off-gas cleaning system optimisation training purposes	Not specified	Not specified	Not specified
Gregoire et al.	2011	Comparison of two modeling approaches to predict variability	Hor air jet approximation	Not specified	DO method
Kocaefe et al.	2013	Different modelling approaches on anode baking furnace	Not mentioned	Not included	Not specified
Baiteche et al.	2015	Effects flue-wall deformation, and employing different radiation models	Empirical kinetic expression	Not included	-P1 -Montecarlo
Ghaui et al.	2016	Implementation of baffleless flue-wall technology	Not mentioned	Not included	Not specified
Zaidani et al.	2017	Effects of flue-wall deformation	Non-reactive flow	Not included	Not specified
Chaodong et al.	2018	Optimisation and development of te furnace structures, process parameters and firing control system	Not specified	Not specified	Not specified
Nakate et al.	2018	Develop a mathematical 2D model to reducing NOx emissions considering turbulent flow, combustion model and radiation	EDM	-$\kappa-\epsilon$ -Spalart-Allmaras	-P1 -DO
Talice	2018	Develop a 2D model to analyse flow behaviour	Not used	- -Spalart-Allmaras	Not used
Talice	2019	Develop a 3D model to analyse flow behaviour	Not used	-$\kappa-\epsilon$	Not used

GMRES is selected (as Krylov subspace method), Algebraic Multigrid (as preconditioner), and Vanka (as pre and post smoother within Algebraic Multigrid).

4.1. Geometry and mesh

Two meshes were created with cfMesh by Prajakta Nakate [4] and one was created with COMSOL Multiphysics. Table 3 presents a description of the ABF geometry and the three meshes. Figure 1 shows the geometry 1 and geometry 2 Additionally, it shows

Preprints (www.preprints.org) | NOT PEER-REVIEWED | Posted: 25 February 2021 doi:10.20944/preprints202102.0565.v1

Table 2. Parameters used to the different models.

Parameter	Model 1	Model 2	Model 3	Model 4	Model 5	Model 6	Model 7	Model 8	Model 9
Fluid properties									
Density (kg/m^3)	1.2	1.2	1.2	1.2	1.2	1.2	1.2	1.2	1.2
Dynamic viscosity (Pa s)	8.9e-4	1.8e-5	8.9e-4	1.8e-5	1.8e-5	1.8e-5	1.8e-5	1.8e-5	1.8e-5
Initial values for Newton's iterations									
U_x (m/s)	70	0	0	70	0	0	0	0	0
U_y (m/s)	0	0	0	0	0	0	0	0	0
U_z (m/s)	0	0	0	0	0	0	0	0	0
Pressure (Pa)	0	0	0	0	0	0	0	0	0
Boundary conditions									
Wall	No slip								
Inlet	Fully developed flow								
Outlet	Pressure								
Air Inlet average velocity U_{av} (m/s)	1	1	1	1	1	1	1	1	1
Pressure outlet (Pa)	0	0	0	0	0	0	0	0	0
Fuel inlet velocity (m/s)	0	0	70	70	70	70	70	70	70
Geometry and mesh									
Geometry	1	1	1	1	2	2	2	2	2
Mesh	1	1	1	1	2	2	3	3	2
Mesh generation tool	cM	cM	cM	cM	cM	cM	CO	CO	cM
Artificial diffusion scheme									
$\delta\ (\mathbf{u}, p)$	Off	Off	Off	Off	Off	0.005	0.25	Off	Off
$\delta\ (\kappa, \epsilon)$	Off	Off	Off	Off	Off	Off	0.25	Off	Off
Results used as initial value									
Initial value	0	0	0	0	0	$\delta = 0.01$ $(\mathbf{u}, p)$	0	M7	M8

Preprints (www.preprints.org) | NOT PEER-REVIEWED | Posted: 25 February 2021 doi:10.20944/preprints202102.0565.v1

a comparison of the location of fuel inlet pipes in the y-axis. Geometry 2 takes advantage of symmetry.

Geometry 1 details about the design and parameters can be found at [6]. The mesh 1, based on geometry 1, was created with cfMesh [4] and is presented in Figure 2 along with the histogram of mesh size.

Geometry 2 details about the design and parameters can be found at [4]. The mesh 2, based on geometry 2, was created with cfMesh [4] and is presented in Figure 3a along with the histogram of mesh size. The mesh 3, based on geometry 2, was created with COMSOL Multiphysics and is presented in Figure 3b along with the histogram of mesh size.

Those histograms are skewness. We can be noted that meshes created using cfMesh have larger frequencies of cells of small size than the one using COMSOL. Moreover, mesh 1 and 2 have refine regions at the combustion zone where air inlet and fuel inlet meet –to the left at the top. A correct mesh element size, in this zone, will allow incoming fuel velocity to be appropriately captured. It implies a representation of an adequate flow in the rest of the areas, taking into account the calculations made according to the border conditions, as shown in Figure 4a of the mesh 2 generated by cfMesh and Figure 4b of the mesh 3 generated by COMSOL.

Table 3. 3D geometry and meshes description.

Mesh	**Mesh 1**	**Mesh 2**	**Mesh 3**
Generator	cfMesh	cfMesh	COMSOL
Symmetry	No	Yes	Yes
Length x-axis (m)	5.5	5.5	5.5
Length y-axis (m)	5	5	5
Length z-axis (m)	1	0.5	0.5
Location of fuel inlet pipes (z-axis) (m)	0.5	0.25	0.25
Cell shape	Cartesian	Cartesian	Tetrahedral

Four turbulent flow simulations were conducted using mesh 1. Parameters are described in Table 2.

Artificial diffusion was added to achieve convergence, experimental tuning at $\delta = 0.025$. Then, We use in a combined manner mesh 2 (cfMesh) and mesh 3 (COMSOL). Firstly, we modelled the turbulent flow using the mesh 3 and artificial diffusion $\delta = 0.25$, achieving convergence at 10^{-3}. Secondly, we modelled the turbulent flow using the mesh 3 and initial values the previous results, achieving convergence at 10^{-5}. Thirdly, we modelled the turbulent flow using the mesh 2 and initial values the previous results, achieving convergence at 10^{-2}.

4.2. Numerical implementation

4.2.1. Finite-element method in CFD

The discretisation in finite element method consists on the following: the solution of partial differential equations requires a discretisation of the computational domain. A visual representation is shown in Figure 5. Some examples are triangles, quadrangles, tetrahedra, prisms o hexahedra [32]. Each entity is called *element* or cell. Each element must have at least another element as a neighbour. Mesh size is an important factor that determines the complexity of the solution to be calculated.

Finite element method has been approached in [33,34] for fluid problems. Additionally, long before the effectiveness of implementing FEM in computational calculations began to be evaluated.

FEM has the following advantages:

1. It is a very-general method

Preprints (www.preprints.org) | NOT PEER-REVIEWED | Posted: 25 February 2021 doi:10.20944/preprints202102.0565.v1

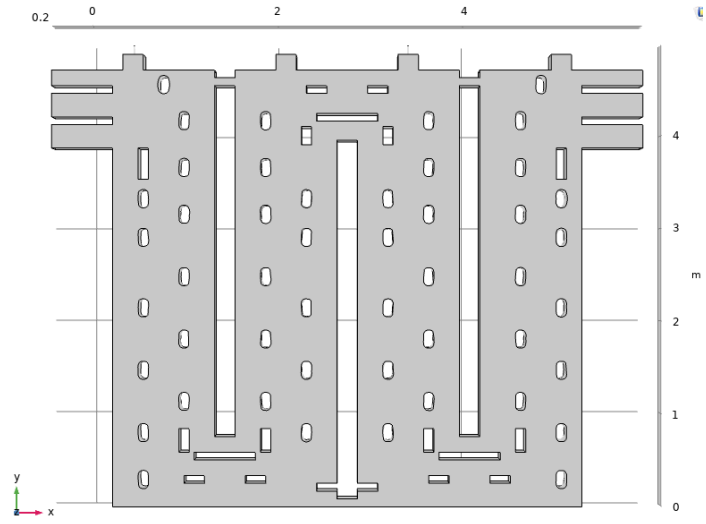

(a) Geometry 1

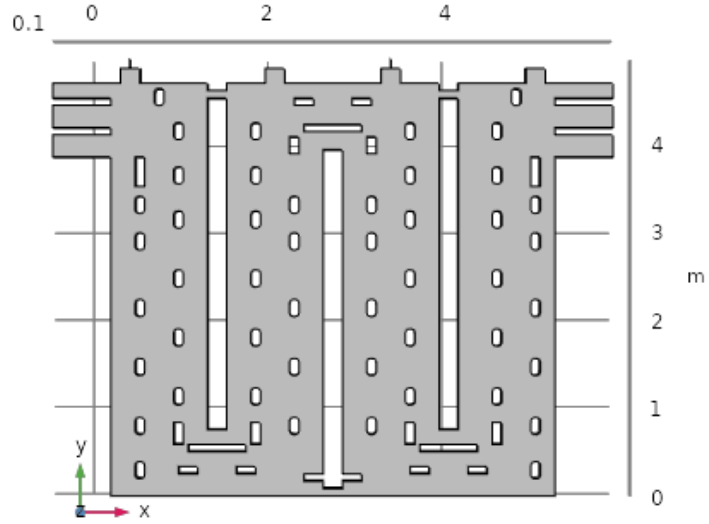

(b) Geometry 2

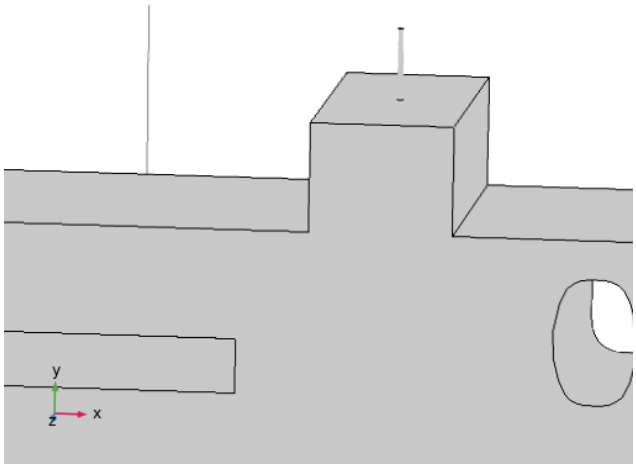

(c) Section at the left fuel inlet pipe zone of geometry 1

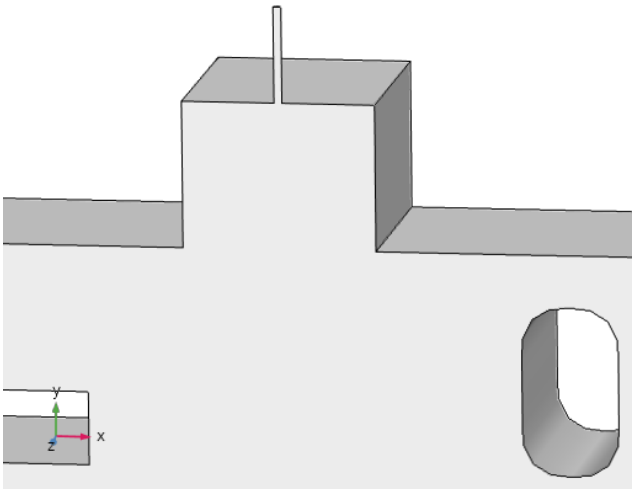

(d) Section at the left fuel inlet pipe zone of geometry 2

Figure 1. Geometry 1 and 2

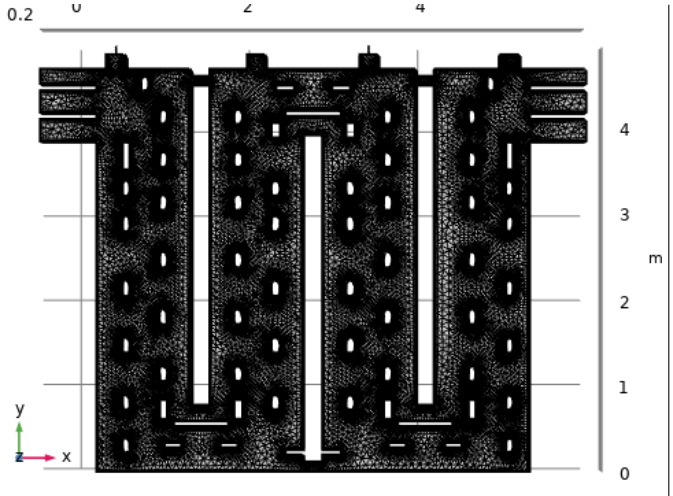

(a) Mesh generated from geometry 1

(b) Histogram of mesh cell size quality

Figure 2. Mesh 1 generated using cfMesh from geometry 1

Preprints (www.preprints.org) | NOT PEER-REVIEWED | Posted: 25 February 2021 doi:10.20944/preprints202102.0565.v1

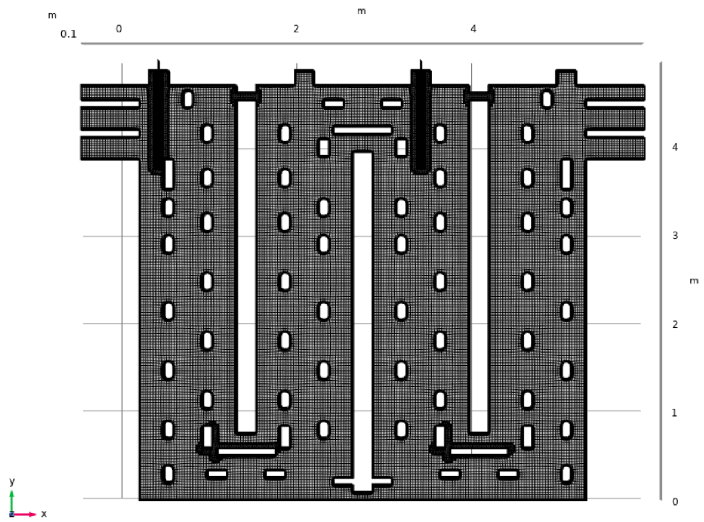

(a) Mesh 2 generated by cfMesh from geometry 2

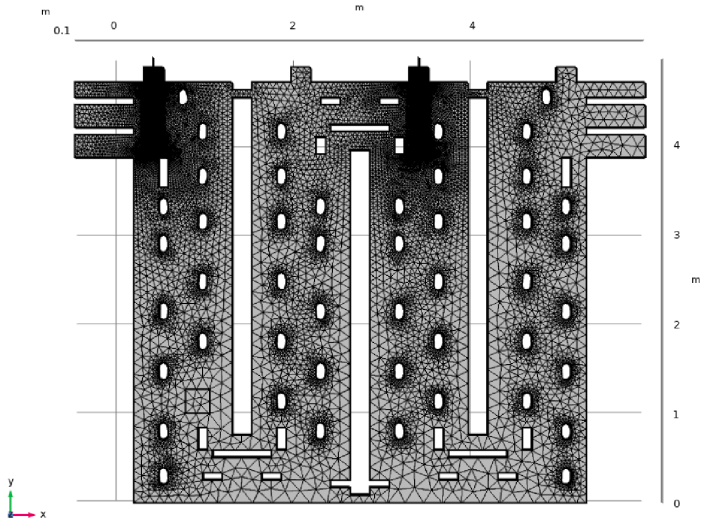

(b) Mesh 3 generated by COMSOL from geometry 2

(c) Histogram of cell size quality of mesh 2 generated by cfMesh from a 3D geometry

(d) Histogram of cell size quality of mesh 3 generated by COMSOL from a 3D geometry

Figure 3. Comparison between histograms of cell size quality of meshes 2 (generated using COMSOL) and mesh 3 (generated using cfMesh).

2. There is more facility to increment element order
3. Physical fields may reproduce more accurately
4. Physics and mathematics often requires different type of functions to each phenomenon. With FEM different phenomenon can be represented at the same time
5. To reach more accuracy, both increase order of polynomials or refine the mesh

As weaknesses, FEM has the requirement to have more computations to represent phenomena at each basic unit [35]

In this work, Finite Element Method is used. For that reason, the next subsection presents a brief introduction about FEM.

4.2.2. Theoretical definition of FEM

Let Ω be the problem domain (i.e., the area limited by the geometry). In 3D, the curvilinear polygon $\Omega \subset \mathbb{R}^3$ with piecewise analytic boundary

$$\partial\Omega = \bigcup_{i=1}^{M} \bar{\Gamma}_i, \tag{10}$$

$\Omega \subset \mathbb{R}^3$ will be a bounded domain with piecewise analytic boundary $\partial\Omega$ consists of faces Γ_1, Γ_2, ..., Γ_M, which are curved polygons in $\mathbb{R}^3$, joined by edges γ_1, ..., γ_{n_e} (curves in $\mathbb{R}^3$ and vertices A_1, A_2, ..., A_{n_w}.

The weak formulation of the Navier-Stokes equations is:

Preprints (www.preprints.org) | NOT PEER-REVIEWED | Posted: 25 February 2021 doi:10.20944/preprints202102.0565.v1

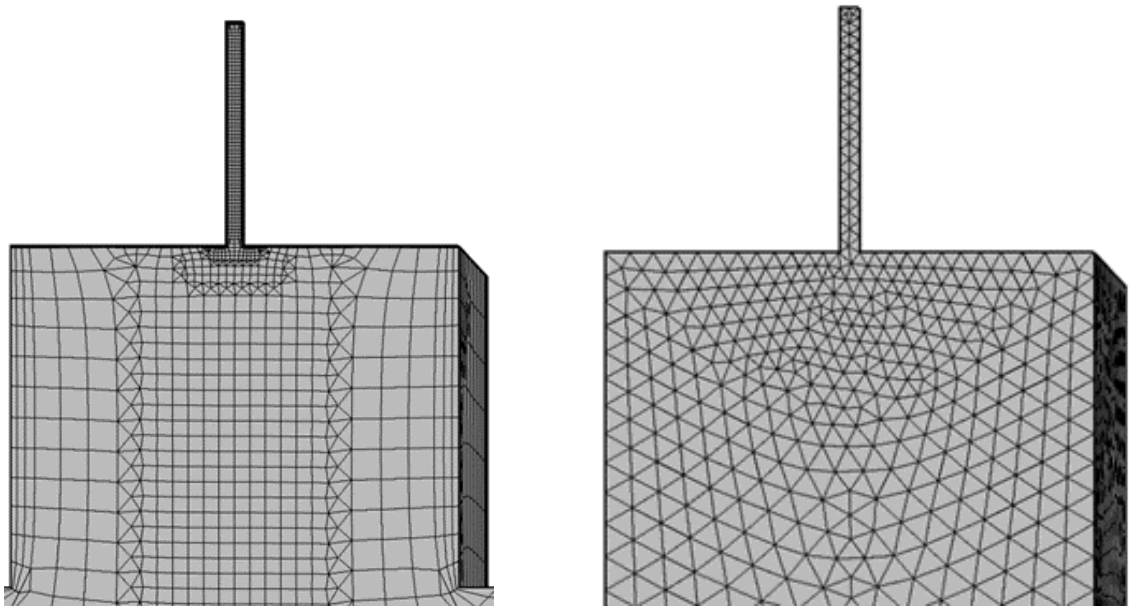

(a) Mesh generated by cfMesh (mesh 2) at the flue inlet zone

(b) Mesh generated by COMSOL (mesh 3) at the flue inlet zone

Figure 4. Comparison between meshes generated using cfMesh (mesh 2) and COMSOL (mesh 3) at the flue inlet zone.

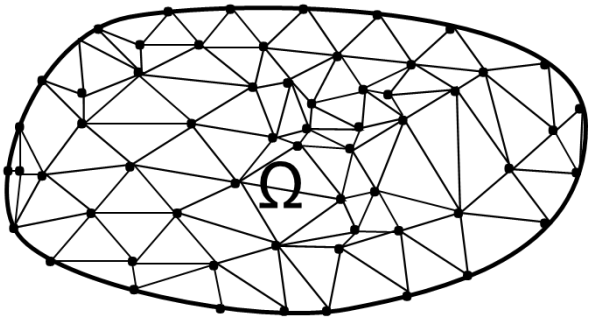

Figure 5. Visual representation of Finite Element Method (FEM) with a finite element triangular mesh.

$$\text{find } \mathbf{u} \in L^2\left(\mathbb{R}^+ \left[H^1(\Omega)\right]^3\right) \cap C^0\left(\mathbb{R}^+ \left[L^2(\Omega)\right]^3\right) \text{ such that:}$$

$$\begin{cases} \int_\Omega \rho \frac{\partial \mathbf{u}}{\partial t} \cdot \boldsymbol{v} + \int_\Omega \mu \nabla \mathbf{u} \cdot \nabla \boldsymbol{v} + \int_\Omega \rho(\mathbf{u} \cdot \nabla)\mathbf{u} \cdot \mathbf{v} - \int_\Omega p \nabla \cdot \mathbf{v} = \int_\Omega \boldsymbol{f} \cdot \mathbf{v} + \int_{\Gamma_N} \boldsymbol{h} \cdot \mathbf{v} \quad \forall \mathbf{v} \in V, \\ \int_\Omega q \nabla \cdot \mathbf{u} = 0 \quad \forall q \in Q. \end{cases} \tag{11}$$

Function $\boldsymbol{h}$ is given Neumann boundaries. $\boldsymbol{f}$ is external force. $\mathbf{v}$ and q are test functions in the space V and Q, respectively. Additional details can be found at [32].

The problem has two variables to approximate, velocity $\mathbf{u}$ and pressure p. So it is known as mixed variational formulation. Solution may be abroad using Lagrange multipliers to determine the value of each variable. However, it is more efficient to use

Preprints (www.preprints.org) | NOT PEER-REVIEWED | Posted: 25 February 2021 doi:10.20944/preprints202102.0565.v1

a penalisation model of p, simplifying the discrete problem to a equations system that only depends on $\mathbf{u}$. This system allows to determine p once calculated $\mathbf{u}$.

In the discretisation problem using FEM, e will be the resulted elements by dividing the domain Ω in the subregions mentioned before. Approximation of unknowns $\mathbf{u} = (u, v, w)$ and p at each element will be given by:

$$u = \sum_{i=1}^{m_u} N_{u_i} q_{u_i} = N_u^T \mathbf{q}_u, \tag{12}$$

$$v = \sum_{i=1}^{m_v} N_{v_i} q_{v_i} = N_v^T \mathbf{q}_v, \tag{13}$$

$$w = \sum_{i=1}^{m_w} N_{w_i} q_{w_i} = N_w^T \mathbf{q}_w, \tag{14}$$

$$p = \sum_{i=1}^{m_p} N_{p_i} q_{p_i} = N_p^T \mathbf{q}_p, \tag{15}$$

where vectors $\mathbf{q}_u$,$\mathbf{q}_v$,$\mathbf{q}_w$, and $\mathbf{q}_p$ denotes local values inside the velocities field $\mathbf{u} = (u, v, w)$ and p of pressure field, respectively. N_u, N_v and N_p are shape functions of the velocity and pressure, and the unknown total vector of element e is given by $\mathbf{q}_e$, i.e, $\mathbf{q}_e^T = [\mathbf{q}_u^T, \mathbf{q}_v^T, \mathbf{q}_w^T, \mathbf{q}_p^T]$.

Unknowns in the problem are no longer mathematical functions and become the value of these functions at the nodes. The complete problem solution follows the rules for discrete problems.

5. Results and discussion

In all the convergence plots, blue and green are related to the convergence reached by the fluid flow (velocity-pressure) and the turbulence ($\kappa - \epsilon$) variables, respectively.

Figure 6 shows the velocity field and the segregated solver plot resulted with the model 1.

The model converged since it reached convergence values around to 10^{-3}. Turbulent flow model describes the fluid flow appropriately according to the set of parameters considered. This fact allows us to observe that a fine mesh is necessary, and hence, higher fluid velocities are allowed.

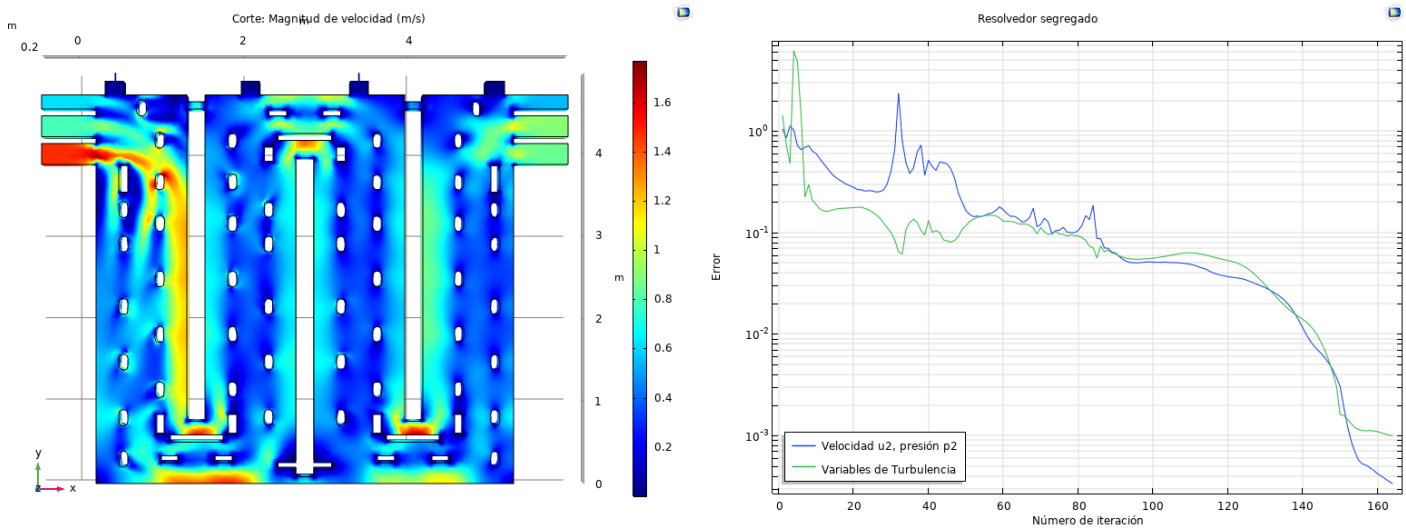

(a) Velocity field **(b)** Segregated solver plot

Figure 6. Model 1: Effects of having velocity 0 and viscosity $8.9e^{-4}$ Pa · s.

Preprints (www.preprints.org) | NOT PEER-REVIEWED | Posted: 25 February 2021 doi:10.20944/preprints202102.0565.v1

The results of the velocity field and segregated solver plot of model 2 are shown in Figure 7. In the velocity field plot, higher velocities are modelled. Small streams with high velocity are seen near the baffles. In fact, it is due to the effect of lowering the viscosity. Convergence plot suggests that the Model 2 is feasible when using low viscosities. Nevertheless, the effect of velocity of fuel is not considered at this stage.

In the same way, figures 8a 8b show the velocity field of the model 3 and the segregated solver plot, respectively. The model has converged which is reached around 10^{-3}.

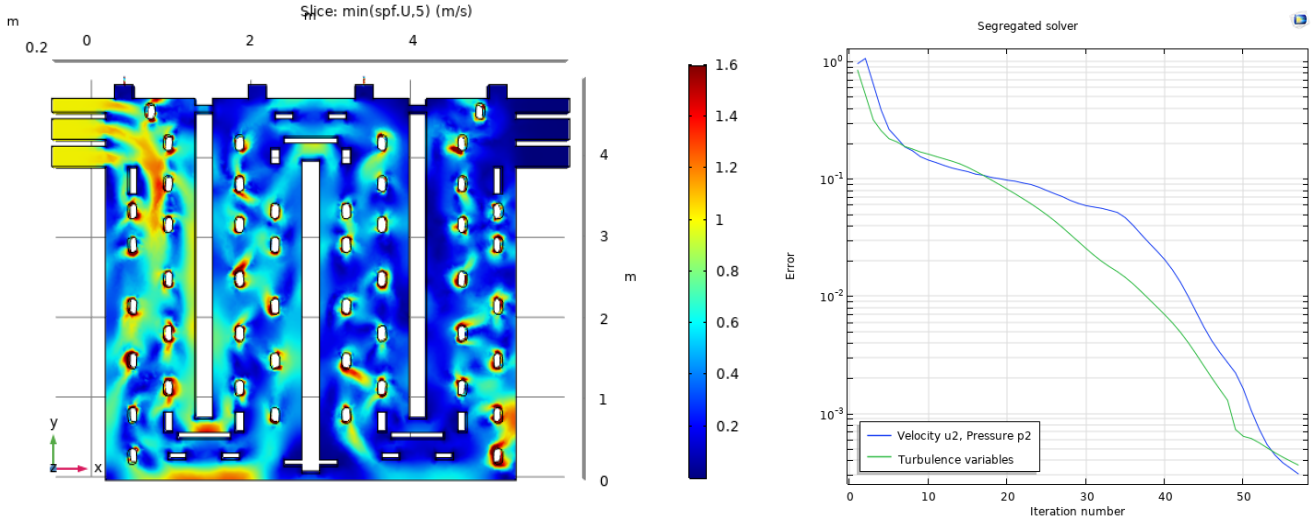

(a) Velocity field **(b)** Segregated solver plot

Figure 7. Model 2: Effects of having velocity 0 and viscosity $1.8e^{-5}$ Pa · s.

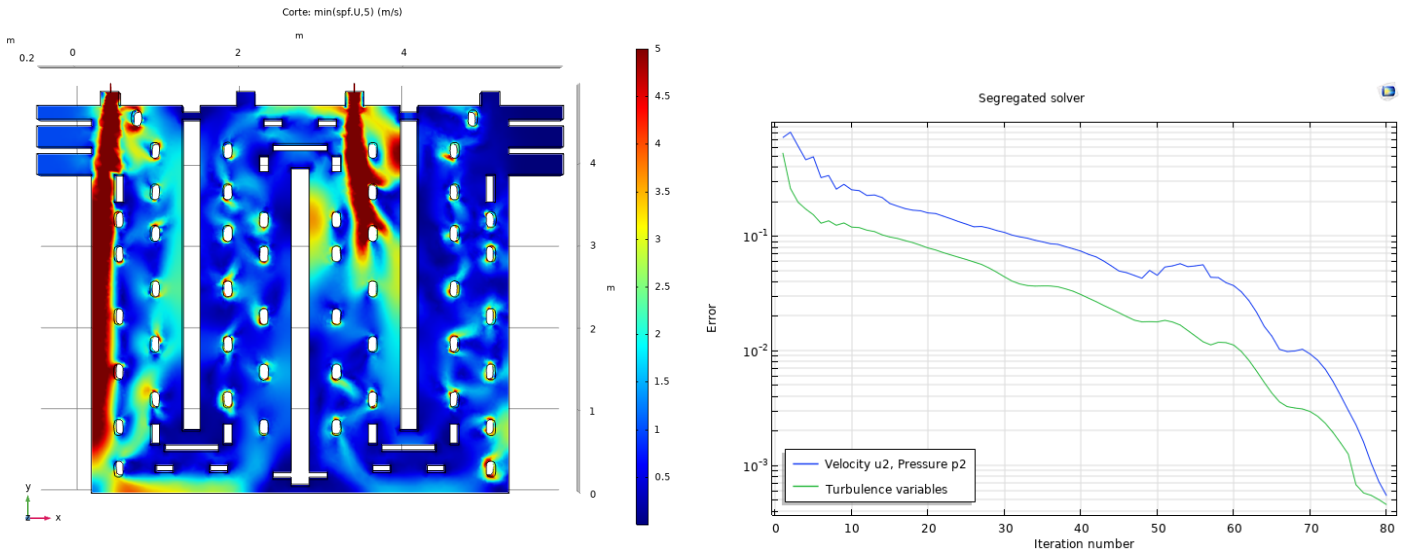

(a) Velocity field **(b)** Segregated solver plot

Figure 8. Model 3: Effects of having velocity $70m/s$ and viscosity $8.9e^{-4}$ Pa · s.

Finally, Figures 9a and 9b show velocity field plot and the segregated solver plots, respectively.

Vanka-AMG-GMRES is optimal for the segregated step that contains the pressure. The other segregated steps are less influential on the overall performance.

Preprints (www.preprints.org) | NOT PEER-REVIEWED | Posted: 25 February 2021 doi:10.20944/preprints202102.0565.v1

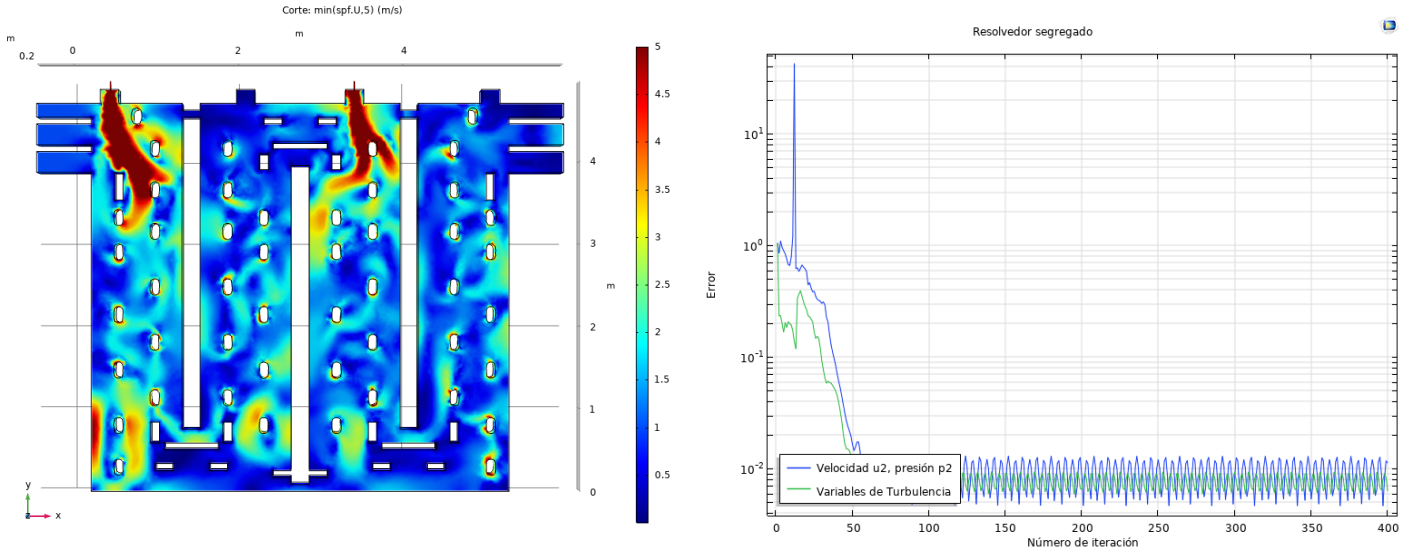

(a) Velocity field **(b)** Segregated solver plot

Figure 9. Model 4: Effects of having velocity $70m/s$ and viscosity $1.8e^{-5}$ Pa · s.

When lowering the viscosity and increasing the velocity, turbulent phenomena appear with long eddies, which represents a chaotic flow. This is not in line with what is expected. Additionally, from the convergence plots, we show that the finite element method used is unstable, and oscillations may occur [36].

We conclude that there is a need to refine the meshes at locations that present a high residuals. Additionally, refinement need to be done in the areas near the fuel inlet pipes and the convergence between the flows from the left inlet pipe and the air inlets.

Figure 10 shows the segregated solver convergence plot of the model 5, showing the turbulent variables and the $\kappa - \epsilon$ variables. The model has not reached the desired convergence of 10^{-3}.

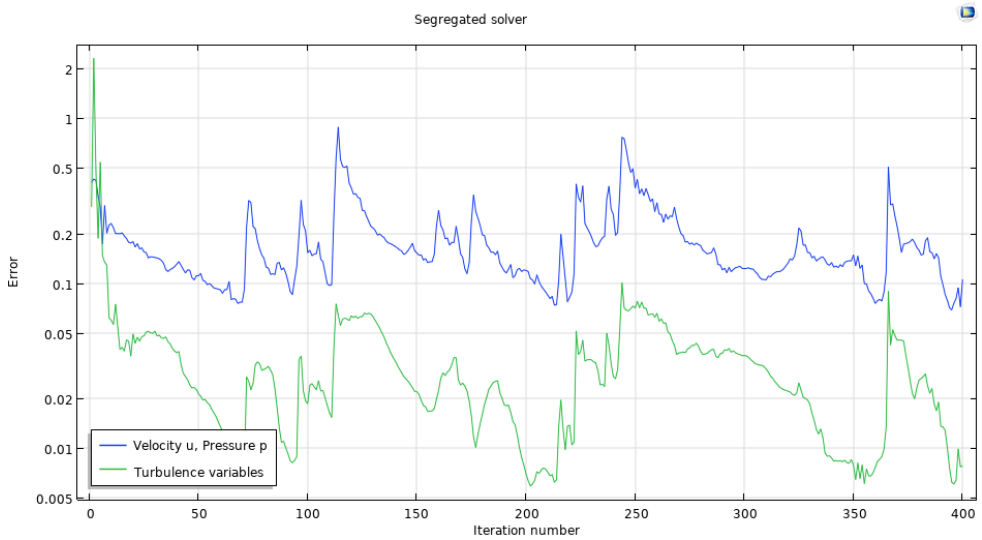

Figure 10. Model 5: Fuel inlet velocity 70m/s. Viscosity $1.8e^{-5}$ Pa · s.

Experimental simulations have shown that no convergence were reached when having the lowest viscosity and the highest velocity required. Using a refined mesh there is an increment the computer load. Additionally, there were repeated oscillations in the convergence plots without showing signs of reaching a value to reaching a minimum error. Lowest error reached was 10^{-1}.

Preprints (www.preprints.org) | NOT PEER-REVIEWED | Posted: 25 February 2021 doi:10.20944/preprints202102.0565.v1

As an alternative, artificial diffusion was added to achieve convergence. In the model 6, Isotropic Diffusion model was used with the tuning parameter $\delta = 0.005$. Figure 11a shows the velocity field using the three components (x, y, z). Lowest error of 10^{-3} was reached. Figure 11b shows the wall resolution in viscous units, as well as Figure 11c shows the residual convergence plot. Figure 11d shows the segregated solver plot of the simulation. Convergence has been reached. However, this has been due to the linearity that has been forced into the model, even the residual plot showing low values (Figure 11c). This represents a false diffusion that is not in accordance with reality. The effect of artificial diffusion can be seen graphically in Figure 11a. The fuel inlet velocity is low, and this is not exact. Therefore, fuel inlet does not penetrate downwards properly. The fluid at the farthest down locations of the section of ABF has not the desired velocities. Despite the above, artificial diffusion scheme is an alternative the cases of high complexity and computational load. Generally, a simulation with artificial diffusion is used as the initial value of a simulation without artificial diffusion [37]. This allows the solver to reach a solution starting from an approximate value of the solution.

Model 7 focuses on the effects of mesh generation on modelling a single section of an ABF using COMSOL mesh generator from an existing geometry, as described in Table 2. In particular, this simulation uses artificial diffusion with the aim of achieving convergence. Figures 12b and 12a present the segregated solver plot and the velocity slide plot. The velocity plot shows that there are thin streams with high velocity. We infer that few high-velocity streams are produced by two factors: 1) errors when generating the mesh using COMSOL with lower cell size in previous models. 2) Low convection due to the increment of diffusion. These are the reasons for having low confidence of these results. Nevertheless, these results can be used as initial values to the next model without any artificial increment of diffusion. Figure 13 show the velocity field and the segregated convergence plot of the model 8. We can observe convergence of the velocity plots. However, graphical results from the velocity field plot (Figure 13a) brings evidence of remaining low-velocity streams near the fuel inlet pipes. We do not have the expected results using the mesh 3, generated by COMSOL.

We believe that there are details to be improved in the implementation of the mesh generator tool, since we obtained the lowest cell-size mesh. Hence, non-trivial geometries representing structures such as an ABF could be meshed using COMSOL in refined areas.

Mesh 2 is the most refined at the required zones. Model 9 used this mesh, and the initial value is the results obtained from the model 8. The lowest error value reached is $2x10^{-2}$ for the $\mathbf{u}$, p and $5x10^{-3}$ for the $k - \epsilon$. Figure 14 shows the velocity slide plot at the iteration with the lowest error value reached, and the convergence solver plot.

When deactivating the artificial diffusion scheme, there is an increment of the velocity in all locations. From Figure 14a, it can be seen the flow stream penetrating with high velocities in ever lower locations. After 400 iterations, it has achieved a maximum error of 10^{-2}. Using an approximate solution approach – even with artificial diffusion – as a starting value of models without false linearity, is still useful for complex studies.

Figure 15 shows a comparison among wall resolution of the models 7, 8, and 9 when using different contributions of isotropic diffusion scheme. It can be seen the effects of artificial diffusion in the wall resolution scheme.

Additionally, as already known, the initial value of the Newton method is determinant on achieving convergence or not. We know that this problem is not smooth in terms of a visual representation of the partial differential equations. It is important at least to approach a high-confident solution and close to reality. We used results of models with simple meshes as input to models with more complex meshes that contributes to have accurate representations with high confidence.

6. Conclusions

In this work, we compared meshes created with cfMesh and COMSOL Multiphysics generator for simulations of turbulent flow in 3D non-trivial geometry.

The turbulent flow in a single section of an ABF was modelled with the $\kappa - \epsilon$ Navier-Stokes equations. Navier-Stokes equations are solved using approximations by numerical methods. In most cases, the limited accuracy is a fair trade-off for the number of computational resources saved compared to using more complicated turbulence models. However, Navier-Stokes approximations using numerical methods are well known for the lack of an exact solution. In this work, we used an approximation provided by Reynolds-Averaged Navier-Stokes.

Analysis of 3D meshes with different mesh cell sizes allowed understanding that the finer the mesh, the better the description of velocity in specific areas.

According to the tests carried out, choosing iterative or segregated solvers may be measured in computational resources (memory, processing capacity, etc.). An example is the use of segregated solvers in contrast to direct solvers, which have a high impact on memory. It is difficult to determine the behaviour of the resulting matrices. Within the Newton iterative process, the influence of one smother or another may not have a preponderant factor in solving the numerical problem. Furthermore, it seems that the choice of one solver or another within a set of candidates for these turbulence models does not guarantee to find or not the desired convergence.

A 3D model becomes numerically unstable when considering large velocities. Large velocities imply larger Reynolds number and the larger Reynolds number the larger inertial forces. Inertial forces are described in the nonlinear term. Due to the variation in time by nature, the $\kappa - \epsilon$ Navier-Stokes problem is transient. COMSOL treats with this problem using pseudo time-stepping. Considering a RANS model – such as $k - \epsilon$– the modelling is feasible to be implemented using computer resources.

We observed that the mesh is the most important factor itself on guarantying convergence. Thus, the most critical areas require of small cell size for capturing the fluid movement accurately. In this way, adaptive mesh sizes have a place within modelling. Refining the mesh in the appropriate locations brings the Peclet number down without false contributions of diffusion.

Cartesian mesh generated using cfMesh describes better the fluid field in the physical sense than the tetrahedral using COMSOL. Problems were found in the built-in COMSOL mesh generation tool in refining non-trivial structures such as an ABF. The use of another external mesh generator may be considered in the future.

Ensuring the optimal and adaptive cell size (i.e, refining the cell size at the appropriate locations and hence do not have the same mesh size at all the domain) imply convergence, correct physical sense, and feasible computational complexity. Important results on this topic are shown by Nakate et al. in [4].

Funding: This work was partially supported by the Delft University of Technology, Delft, The Netherlands.

Conflicts of Interest: The authors declare no conflict of interest.

Acknowledgments: The first author acknowledges the Delft University of Technology for the partial funding for this project. Also, the first author express his acknowledgement to the Bioinformatic Research Group at the *Universidad del Valle* for providing access to the HPC cluster, and to Mayra Alvear for additional help in theoretical background.

Preprints (www.preprints.org) | NOT PEER-REVIEWED | Posted: 25 February 2021 doi:10.20944/preprints202102.0565.v1

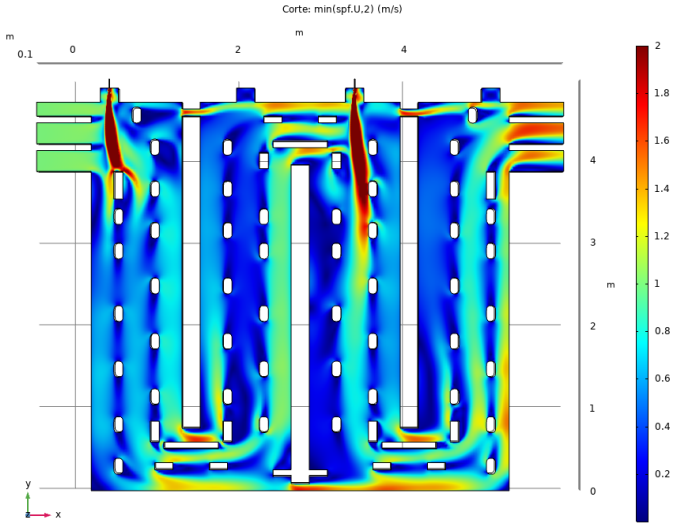

(a) Velocity field

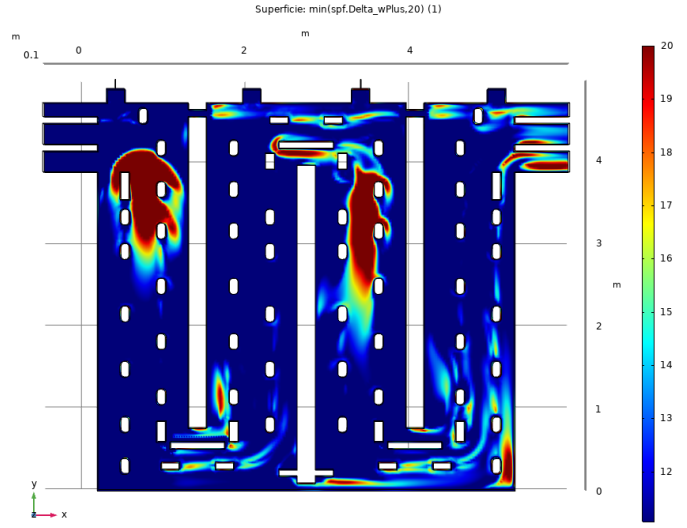

(b) Wall resolution in viscous units

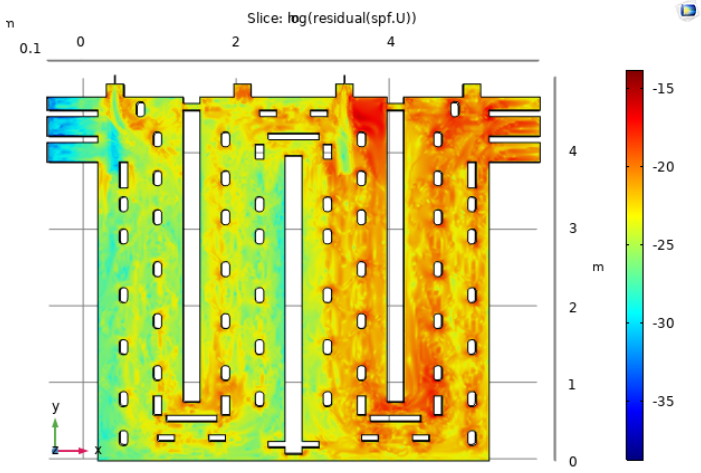

(c) Residual plot

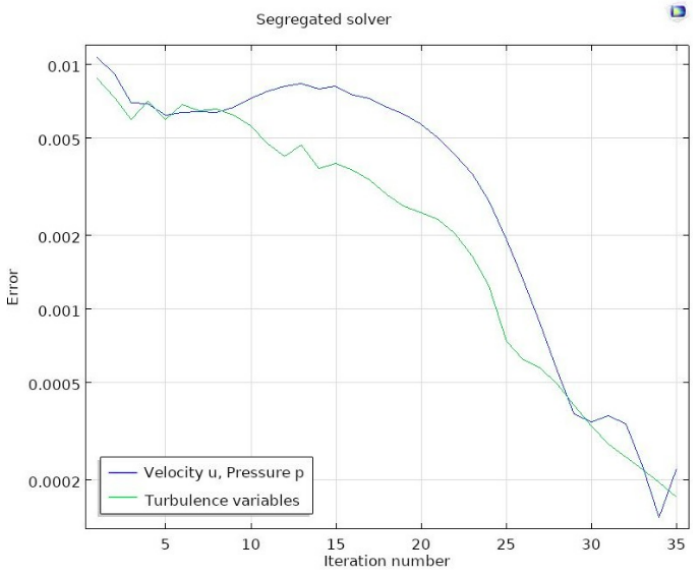

(d) Segregated solver plot

Figure 11. Model 6: results using isotropic diffusion with $\delta = 0.5$. Fuel inlet velocity 70m/s. Viscosity $1.8e^{-5}$ Pa · s.

Preprints (www.preprints.org) | NOT PEER-REVIEWED | Posted: 25 February 2021 doi:10.20944/preprints202102.0565.v1

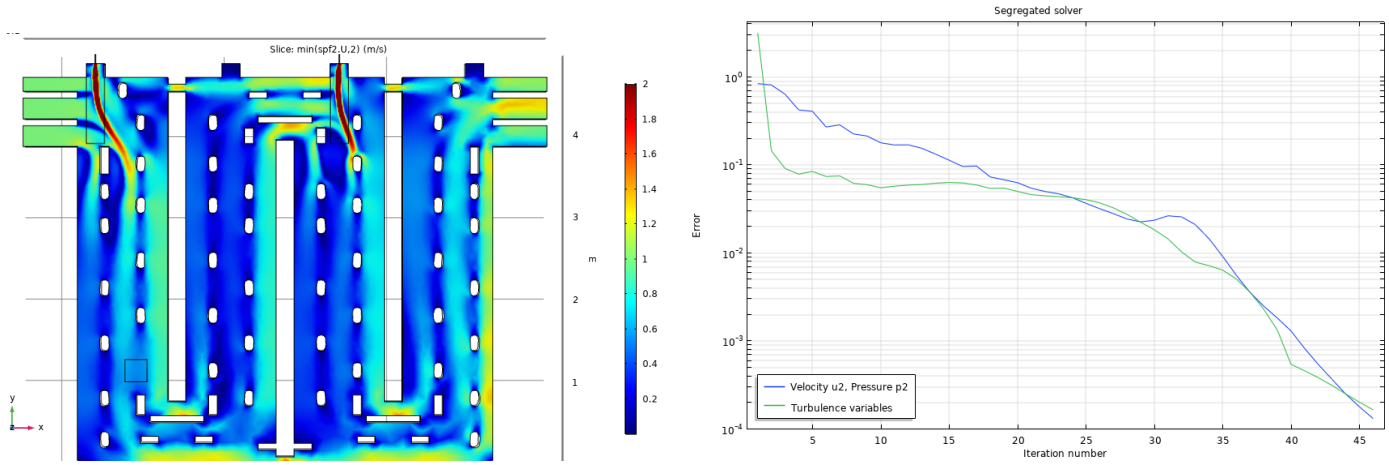

(a) Velocity slide plot **(b)** Segregated solver plot

Figure 12. Model 7: artificial diffusion $\delta = 0.25u, p, k, \epsilon$ using mesh 3 generated by COMSOL. Initial Value for Newton method: Zero.

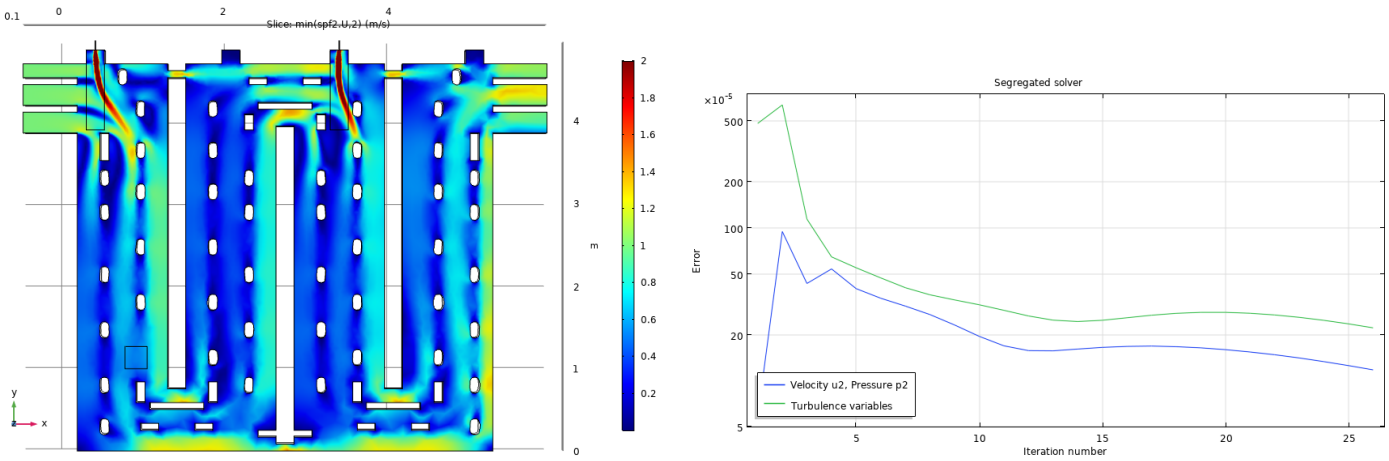

(a) Velocity slide plot **(b)** Segregated solver plot

Figure 13. Model 8: No artificial diffusion using mesh 3 generated by COMSOL. Initial Value for Newton method: results of model 7.

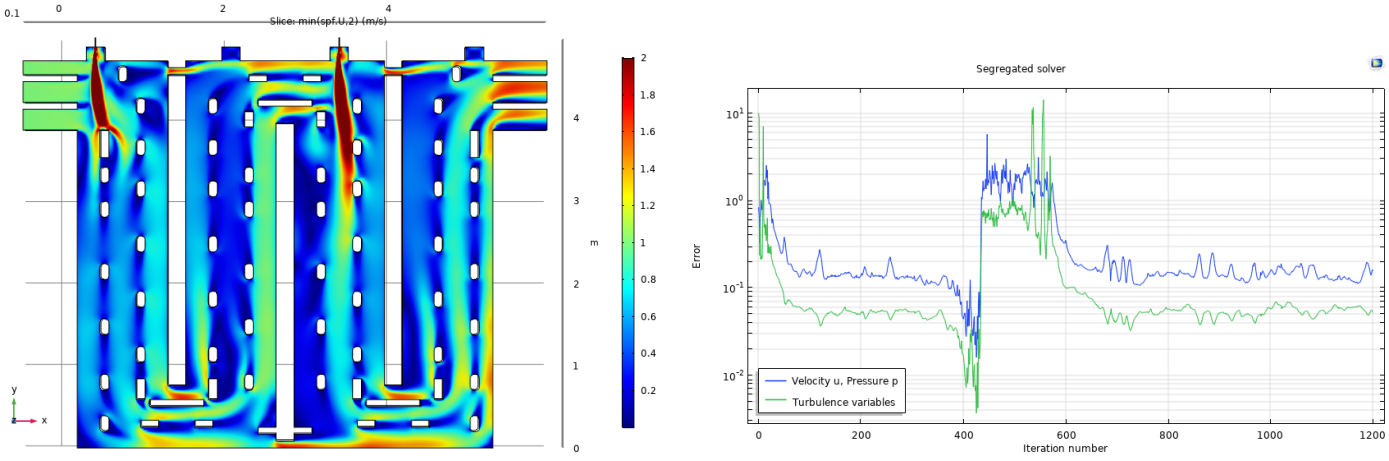

(a) Velocity slide plot **(b)** Segregated solver plot

Figure 14. Model 9: No artificial diffusion using mesh 2 generated by cfMesh. Initial Value for Newton method: results of model 8.

Preprints (www.preprints.org) | NOT PEER-REVIEWED | Posted: 25 February 2021 doi:10.20944/preprints202102.0565.v1

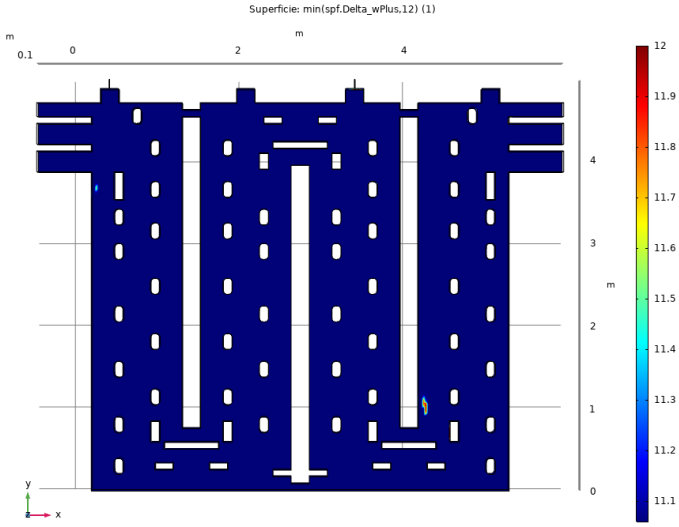

(a) Wall resolution. Artificial diffusion with $\delta = 0.5$

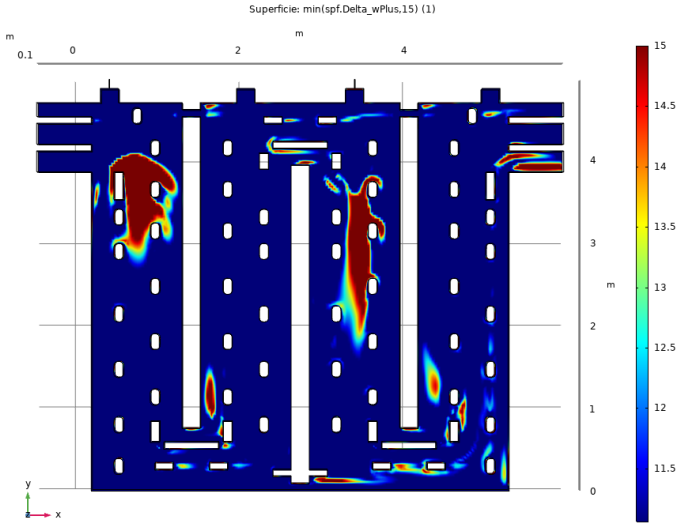

(b) Wall resolution. Artificial diffusion with $\delta = 0.05$

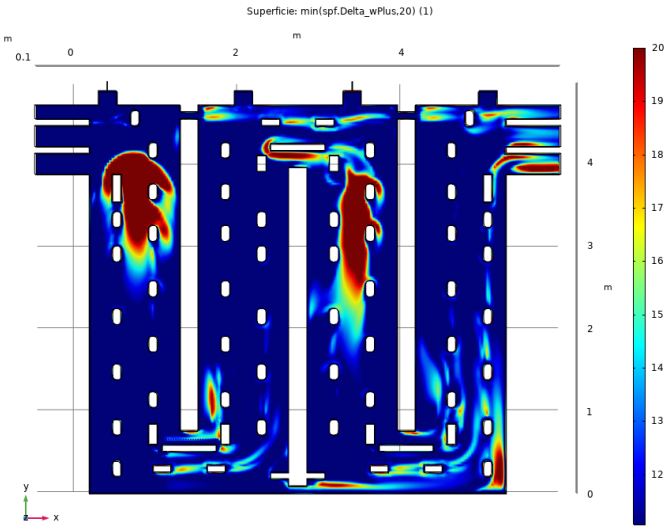

(c) Wall resolution. Artificial diffusion with $\delta = 0.005$

Figure 15. Comparison among wall resolution plots with different values of isotropic diffusion δ. Inlet velocity: 70m/s. Viscosity $1.8e-5$. Mesh 2 generated using cfMesh

 doi:10.20944/preprints202102.0565.v1

References

1. Severo, D.S.; Gusberti, V. User-friendly software for simulation of anode baking furnaces. Proceeding of the 10th Australasian Aluminum Smelting Technology Conference, 2011.
2. Mahieu, P.; Sedmak, P. Improving fuel gas injection in anode baking furnace. In *Light Metals 2014*; Springer, 2014; pp. 1165–1169.
3. Directive, C. Directive 2010/75/EU of the European Parliament and of the Council. *Off. J. Eur. Union L* **2010**, *334*, 17–119.
4. Nakate, P.; Lahaye, D.; Vuik, C.; Talice, M. Analysis of the aerodynamics in the heating section of an anode baking furnace using non-linear finite element simulations. *Fluids* **2021**, *6*, 46.
5. Tajik, A.R.; Shamim, T.; Al-Rub, R.K.A.; Zaidani, M. Performance analysis of a horizontal anode baking furnace for aluminum production. ICTEA: International Conference on Thermal Engineering, 2017, Vol. 2017.
6. Nakate, P.; Lahaye, D.; Vuik, C.; Talice, M. Computational study of the anode baking industrial furnace.
7. Nakate, P.; Lahaye, D.; Vuik, C. Numerical Modeling of Anode Baking Furnace with COMSOL Multiphysics® **2018**.
8. Talice, M. TU-Delft Technical Report Report 01/2018. Technical report, PMSQUARED Engineering, 2018.
9. Severo, D.S.; Gusberti, V.; Pinto, E.C. Advanced 3D modelling for anode baking furnaces. *Light Metals* **2005**, *2005*, 697–702.
10. Keller, F.; Mannweiler, U.; Severo, D. Computational Modeling in Anode Baking. 2006.
11. Goede, F. Refurbishment and modernization of existing anode baking furnace. *Light Metals* **2007**, *1984*, 973–976.
12. Bui, R.; Dernedde, E.; Charette, A.; Bourgeois, T. Mathematical simulation of a horizontal flue ring furnace. In *Essential Readings in Light Metals*; Springer, 2016; pp. 386–389.
13. Kocaefe, Y.; Dernedde, E.; Kocaefe, D.; Ouellet, R.; Jiao, Q.; Crowell, W. A 3D mathematical model for the horizontal anode baking furnace. Technical report, Minerals, Metals and Materials Society, Warrendale, PA (United States), 1996.
14. Severo, D.S.; Gusberti, V.; Sulger, P.O.; Keller, F.; Meier, M.W. Recent developments in anode baking furnace design. In *Light Metals 2011*; Springer, 2011; pp. 853–858.
15. Zhou, P.; Mei, C.; Zhou, J.m.; Zhou, N.j.; Xu, Q.h. Simulation of the influence of the baffle on flowing field in the anode baking ring furnace. *Journal of Central South University of Technology* **2002**, *9*, 208–211.
16. Ordronneau, F.; Gendre, M.; Pomerleau, L.; Backhouse, N.; Berkovich, A.; Huang, X. Meeting the challenge of increasing anode baking furnace productivity. In *Light Metals 2011*; Springer, 2011; pp. 865–870.
17. Baiteche, M.; Kocaefe, D.; Kocaefe, Y.; Marceau, D.; Morais, B.; Lafrance, J. Description and applications of a 3D mathematical model for horizontal anode baking furnaces. In *Light Metals 2015*; Springer, 2015; pp. 1115–1120.
18. Zaidani, M.; Al-Rub, R.A.; Tajik, A.R.; Shamim, T. 3D Multiphysics model of the effect of flue-wall deformation on the anode baking homogeneity in horizontal flue carbon furnace. *Energy Procedia* **2017**, *142*, 3982–3989.
19. Kocaefe, Y.; Oumarou, N.; Baiteche, M.; Kocaefe, D.; Morais, B.; Gagnon, M. Use of mathematical modelling to study the behavior of a horizontal anode baking furnace. In *Light Metals 2013*; Springer, 2016; pp. 1139–1144.
20. Valen-Sendstad, K.; Mortensen, M.; Langtangen, H.P.; Reif, B.; Mardal, K.A. Implementing a k-epsilon Turbulence Model in the FEniCS Finite Element Programming Environment. 2013.
21. Oumarou, N.; Kocaefe, D.; Kocaefe, Y.; Morais, B. Transient process model of open anode baking furnace. *Applied Thermal Engineering* **2016**, *107*, 1253–1260.
22. Oumarou, N.; Kocaefe, D.; Kocaefe, Y. An advanced dynamic process model for industrial horizontal anode baking furnace. *Applied Mathematical Modelling* **2018**, *53*, 384–399.
23. Oumarou, N.; Kocaefe, Y.; Kocaefe, D.; Morais, B.; Lafrance, J. A dynamic process model for predicting the performance of horizontal anode baking furnaces. In *Light Metals 2015*; Springer, 2015; pp. 1081–1086.
24. Tajik, A.R.; Shamim, T.; Al-Rub, R.K.A.; Zaidani, M. Two dimensional CFD simulations of a flue-wall in the anode baking furnace for aluminum production. *Energy Procedia* **2017**, *105*, 5134–5139.
25. Tajik, A.R.; Shamim, T.; Zaidani, M.; Al-Rub, R.K.A. The effects of flue-wall design modifications on combustion and flow characteristics of an aluminum anode baking furnace-CFD modeling. *Applied Energy* **2018**, *230*, 207–219.
26. L, C.; C, Y.; Z, S.; X, H.; S, Y. Research and application for large scale, high efficiency and energy saving baking furnace technology. TMS annual meeting exhibition, 2018.
27. El Ghaoui, Y.; Besson, S.; Drouet, Y.; Morales, F.; Tomsett, A.; Gendre, M.; Anderson, N.M.; Eich, B. Anode baking furnace fluewall design evolution: a return of experience of latest baffleless technology implementation. In *Light Metals 2016*; Springer, 2016; pp. 941–945.
28. Talice, M. TU-Delft Technical Report Report 01/2019. Technical report, PMSQUARED Engineering, 2019.
29. Gregoire, F.; Gosselin, L.; Alamdari, H. Sensitivity of carbon anode baking model outputs to kinetic parameters describing pitch pyrolysis. *Industrial & Engineering Chemistry Research* **2013**, *52*, 4465–4474.
30. Grégoire, F.; Gosselin, L. Comparison of three combustion models for simulating anode baking furnaces. *International Journal of Thermal Sciences* **2018**, *129*, 532–544.
31. Wilcox, D. *Turbulence Modeling for CFD, 2nd ed.*; Vol. 2, DCW Industries, 1998.
32. Quarteroni, A.; Quarteroni, S. *Numerical models for differential problems*; Vol. 2, Springer, 2009.
33. Krizek, M.; Neittaanmaki, P.; Stenberg, R. *Finite element methods: fifty years of the Courant element*; CRC Press, 2016.
34. Donea, J.; Huerta, A. *Finite element methods for flow problems*; John Wiley & Sons, 2003.
35. Ferziger, J.H.; Perić, M.; Street, R.L. *Computational methods for fluid dynamics*; Vol. 3, Springer, 2002.
36. Wegner, J.; Ganzer, L. Numerical simulation of oil recovery by polymer injection using COMSOL. Excerpt from the Proceedings of the 2012 COMSOL Conference Milan, 2012.
37. Understanding Stabilization Methods. https://www.comsol.com/blogs/understanding-stabilization-methods/. Accessed: 2020-08-01.